

Compound Defects in Halide Perovskites: A First-Principles Study of CsPbI₃

Haibo Xue,^{†,‡} José Manuel Vicent-Luna,^{†,‡} Shuxia Tao,^{*,†,‡} and Geert
Brocks^{*,†,‡,¶}

[†]*Materials Simulation & Modelling, Department of Applied Physics, Eindhoven University
of Technology, P.O. Box 513, 5600MB Eindhoven, the Netherlands.*

[‡]*Center for Computational Energy Research, Department of Applied Physics, Eindhoven
University of Technology, P.O. Box 513, 5600MB Eindhoven, the Netherlands.*

[¶]*Computational Materials Science, Faculty of Science and Technology and MESA+
Institute for Nanotechnology, University of Twente, P.O. Box 217, 7500AE Enschede, the
Netherlands.*

E-mail: s.x.tao@tue.nl; g.h.l.a.brocks@utwente.nl

Abstract

Lattice defects affect the long-term stability of halide perovskite solar cells. Whereas simple point defects, i.e., atomic interstitials and vacancies, have been studied in great detail, here we focus on compound defects that are more likely to form under crystal growth conditions, such as compound vacancies or interstitials, and antisites. We identify the most prominent defects in the archetype inorganic perovskite CsPbI_3 , through first-principles density functional theory (DFT) calculations. We find that under equilibrium conditions at room temperature, the antisite of Pb substituting Cs forms in a concentration comparable to those of the most prominent point defects, whereas the other compound defects are negligible. However, under nonequilibrium thermal and operating conditions, other complexes also become as important as the point defects. Those are the Cs substituting Pb antisite, and, to a lesser extent, the compound vacancies of PbI_2 or CsPbI_3 units, and the I substituting Cs antisite. These compound defects only lead to shallow or inactive charge carrier traps, which testifies to the electronic stability of the halide perovskites. Under operating conditions with a quasi Fermi level very close to the valence band, deeper traps can develop.

Introduction

On the basis of their outstanding efficiency (25.7% to date¹) and relative ease of fabrication, halide perovskite solar cells seem to be poised for large scale applications. The primary obstacle blocking their present commercialization is their relative rapid degradation under operating conditions.²⁻⁵ On a microscopic level, lattice defects in the perovskite materials initiate the degradation process, as they facilitate migration of ions,⁶⁻¹⁰ chemical reactions,^{11,12} phase transitions,¹³ and phase segregation.¹⁴

Because of the experimental difficulties in characterizing defect structures microscopically, much of our current understanding of lattice defects in halide perovskites stems from results obtained from electronic structure calculations based on density functional theory

(DFT). Following common semiconductor practice,^{15,16} elementary defects consisting of single atomic interstitials, vacancies, or antisites have been at the center of interest.¹⁷⁻²¹ In a previous work,²² we have studied vacancy and interstitial point defects in six primary Pb- and Sn-based halide perovskites with different cations (Cs, MA, FA) and anions (I, Br, Cl), within a single computational framework.²³ One prevalent conclusion from most of these computational studies is that in these materials the points defects with the highest concentrations under equilibrium growth conditions, only introduce shallow traps.

Defects in halide perovskites with a more complex structure have also been considered.²⁴⁻²⁶ Conceptually, such complex defects can be thought of as resulting from a recombination of simple atomic point defects (vacancies or interstitials) to, for instance, PbI_2 or MAI compound vacancies in MAPbI_3 .²⁴⁻²⁶ Within this line of thought also antisites can be interpreted as compound defects, resulting from a recombination of an interstitial and a vacancy of different species. For instance, in CsPbI_3 , cation antisites result from a recombination of a Cs vacancy (interstitial) and an Pb interstitial (vacancy).²⁰ Some compound defects have been predicted to form shallow defects only,^{20,25} whereas others have the potential to form deep traps.^{24,27}

The formation energy of compound defects is typically much higher than that of simple point defects, which implies that under normal equilibrium conditions (room temperature, atmospheric pressure) the concentration of compound defects, including antisites, is negligible.¹⁵⁻¹⁸ However, many crystal growth conditions are highly nonequilibrium, and defects can be formed during growth in appreciable concentrations.²² In molecular dynamics simulations that use a reactive force field,^{10,28} applied to halide perovskites containing an appreciable amount of point defects, one often observes recombination of the latter to compound defects. From positron annihilation lifetime spectroscopy, assisted by DFT calculations, there is evidence of charge carrier trapping at compound vacancy defects in MAPbI_3 .²⁶

In this paper, we study compound defects, vacancies, interstitials and antisites, in the archetype inorganic perovskite CsPbI_3 by means of first-principles DFT calculations. Not

only do we calculate their equilibrium concentrations, but explicitly considering the possible recombination reactions of elementary point defects, we also assess their concentrations under nonequilibrium conditions. The effect of these compound defects on the electronic properties is examined, in particular their potential to form deep traps.

Computational Methods

DFT calculations

Density functional theory (DFT) calculations are performed with the Vienna *Ab-Initio* Simulation Package (VASP),²⁹⁻³¹ employing the SCAN+rVV10^{23,32} functional for electronic calculations and geometry optimization. Our calculations use a plane wave kinetic energy cutoff of 500 eV and a Γ -point-only \mathbf{k} -point mesh. The energy and force convergence criteria are set to 10^{-4} eV and 0.02 eV/Å, respectively. Spin-orbit coupling is omitted, as it has little effect on the formation energies of defects.²³ Spin polarization is included in all calculations.

As in our previous work,²² point defects or compound defects are created in a $2 \times 2 \times 2$ orthorhombic supercell of CsPbI₃, which contains 32 formula units. The lattice volume and ionic positions of the pristine supercell are fully relaxed. Within the supercell, atomic positions of defective structures are optimized. For antisite defects, we use the notation A_B to indicate that atom A substitutes atom B in the lattice. We consider twelve different compound complexes, i.e., the three compound vacancies $V_{[\text{CsI}]}$, $V_{[\text{PbI}_2]}$, and $V_{[\text{CsPbI}_3]}$, the two compound interstitials $[\text{CsI}]_i$ and $[\text{PbI}_2]_i$, the six antisites Cs_I , I_{Cs} , Cs_{Pb} , Pb_{Cs} , Pb_I , and I_{Pb} , and the compound antisite $[2\text{Cs}]_{\text{Pb}}$.

Defect Formation Energy

Under equilibrium conditions, the concentrations of lattice defects can be obtained from Boltzmann statistics

$$\frac{c(D^q)}{c_0(D^q) - c(D^q)} = \exp \left[-\frac{\Delta H_f(D^q)}{k_B T} \right], \quad (1)$$

where D^q indicates the type of defect, either a simple interstitial or vacancy point defect, or a compound interstitial or vacancy, or an antisite defect, with charge q ; c is the defect concentration, and c_0 is the density of possible sites for that particular defect (including orientational degrees of freedom if the defect is not spherically symmetric), where usually $c \ll c_0$; ΔH_f is the defect formation energy (DFE), T is the temperature, and k_B is the Boltzmann constant.

Different types of defects have different charges, but if no external charges are injected, then as a whole a material has to be charge neutral

$$p - n + \sum_{D^q} q c(D^q) = 0, \quad (2)$$

where p and n are the intrinsic charge densities of holes and electrons of the semiconductor material. The charge neutrality condition, Eq. (2), fixes the intrinsic Fermi level.

The DFE is calculated from the expression¹⁵

$$\begin{aligned} \Delta H_f(D^q) = & E_{\text{tot}}(D^q) - E_{\text{bulk}} - \sum_k n_k \mu_k \\ & + q(E_F + E_{\text{VBM}} + \Delta V), \end{aligned} \quad (3)$$

where E_{tot} and E_{bulk} are the DFT total energies of the defective and pristine supercells, respectively, and n_k and μ_k are the number of atoms and chemical potential of atomic species k added to ($n_k > 0$) or removed from ($n_k < 0$) the pristine supercell in order to create the defect. We use the chemical potentials μ_k ; $k = \text{Cs, Pb, I}$, as determined for I-medium conditions in our previous work.²²

Creating a charge q requires taking electrons from or adding them to a reservoir at a fixed Fermi level. The latter is calculated as $E_F + E_{\text{VBM}}$, with $0 \leq E_F \leq E_g$, the band gap, and E_{VBM} the energy of the valence band maximum. As it is difficult to determine the latter from a calculation on a defective cell, one establishes E_{VBM} in the pristine cell, shifted by ΔV , which is calculated by lining up the core level on an atom in the pristine and the neutral defective cell that is far from the defect.^{15,33} The supercell in the calculation and the dielectric screening in CsPbI₃ are sufficiently large, so that the electrostatic interaction between a charged point defect and its periodically repeated images can be neglected.^{19,22,23} In addition, we neglect vibrational contributions to the DFEs, and the effect of thermal expansion on the DFEs, as these are typically small in the present compounds.^{23,34}

Recombination Reaction

We model the recombination of point defects A_1, \dots, A_m to a compound defect B as a chemical reaction



Reaction equilibrium is defined by

$$\sum_{i=1}^m \alpha_i \mu_i = \beta \mu_B, \quad (5)$$

with μ_i and μ_B the chemical potentials of species A_i and B , given by

$$\mu_i = \Delta H_f(A_i^{q_i}) + k_B T \ln \frac{c_i}{c_{0,i} - c_i}; \quad i = 1, \dots, m; \quad (6)$$

$$\mu_B = \Delta H_f(B^{q_B}) + k_B T \ln \frac{c_B}{c_{0,B} - c_B}, \quad (7)$$

where $\Delta H_f(D^q)$; $D^q = A_i^{q_i}, B^{q_B}$ are the DFEs according to Eq. (3), $c_i = c(A_i^{q_i})$, $c_B = c(B^{q_B})$ are concentrations, and $c_{0,i} = c_0(A_i^{q_i})$, $c_{0,B} = c_0(B^{q_B})$ are the densities of possible sites (see Table S1 of the Supporting Information for details). Note that we do not assume that

charge is conserved in reaction (4). The electron reservoir with Fermi energy E_F can supply electrons or holes, which is accounted for in the DFEs. Equations (5)-(7) give the law of mass action

$$\left(\frac{c_B}{c_{0,B} - c_B}\right)^\beta \prod_{i=1}^m \left(\frac{c_{0,i} - c_i}{c_i}\right)^{\alpha_i} = \exp\left[-\frac{\Delta H_r}{k_B T}\right], \quad (8)$$

$$\Delta H_r = \beta \Delta H_f(B^{q_B}) - \sum_{i=1}^m \alpha_i \Delta H_f(A_i^{q_i}), \quad (9)$$

where ΔH_r is the reaction energy of reaction (4).

If all (simple and compound) defects are in equilibrium with reservoirs at chemical potentials μ_k , Eq. (3), then their concentrations are given by Eq. (1), and trivially obey the law of mass action, Eq. (8). Typically, however, point defects and compound defects are initially created at concentrations $c_i^{(0)}$ and $c_B^{(0)}$, respectively, in a crystal growth process, after which the crystals are extracted and kept at room temperature. The defects then remain, but they can recombine according to Eq. (4). Not only does this include the possible formation of compound interstitials or vacancies, but also the formation of antisites through the recombination of an interstitial and a vacancy.

As the recombination reaction, Eq. (4), conserves the total number of atoms of each species, one has

$$c_i + \frac{\alpha_i}{\beta} c_B = c_i^{(0)} + \frac{\alpha_i}{\beta} c_B^{(0)}; \quad i = 1, \dots, m. \quad (10)$$

Given the initial concentrations $c_i^{(0)}$ and $c_B^{(0)}$, the law of mass action, Eq. (8), then allows for determining the actual concentrations of the compound defect c_B , and of the point defects c_i .

Charge State Transition Level

Under operating conditions, charges are injected in the material, shifting the positions of the (quasi) Fermi levels for electrons and holes. The charge state transition level (CSTL) $\varepsilon(q/q')$ is defined as the Fermi level position where the charge states q and q' of the same

type of defect have equal formation energy, $\Delta H_f(D^q) = \Delta H_f(D^{q'})$. As the DFEs have a simple linear dependence on E_F , Eq. (3), this condition can be expressed as

$$\varepsilon(q/q') = \frac{\Delta H_f(D^q, E_F = 0) - \Delta H_f(D^{q'}, E_F = 0)}{q' - q}, \quad (11)$$

where $\Delta H_f(D^q, E_F = 0)$ is the DFE calculated at $E_F = 0$. The CSTLs are important for the electronic properties; if these levels are deep inside the band gap, they can trap charge carriers, and act as nonradiative recombination centers.

The band gap calculated with SCAN+rVV10 suffers from the DFT band gap error. However, we would argue that the positions of the CSTLs with respect to the band edges are correct, because the defects' electronic states have a character similar to either the valence band or the conduction band.³⁵ For a more detailed discussion, see Ref. 22.

Results and discussion

Equilibrium Conditions

Formation of compound defects in semiconductors is often driven by the attractive electrostatic interaction between defects with opposite charge states.^{15,16} Possible compound vacancies in CsPbI₃, resulting from recombination of the point vacancies V_{Cs}^- , V_{Pb}^{2-} and V_{I}^+ , are then V_{CsI} , V_{PbI_2} and $V_{[\text{CsPbI}_3]}$, where the neutral state indeed turns out to be the most stable charge state under intrinsic conditions. Optimized structures of these defects are shown in Figures 1(a-c).

Following the same reasoning, we find the neutral compound interstitial defects $[\text{CsI}]_i$ and $[\text{PbI}_2]_i$, shown in Figures 1(d,e) through recombination of the point interstitials Cs_i^+ , Pb_i^{2+} , and I_i^- . For larger potential compound interstitials, such as $[\text{CsPbI}_3]_i$, we found that the lattice becomes too distorted and the DFE becomes very large.

Formation energies of the compound vacancies and interstitials, calculated according to

Eq. (3), are shown in Figures 2(a,b). Taking into account of all point defects and compound defects, the intrinsic Fermi level, $E_F^{(i)}$, calculated with the charge neutrality condition, Eq. (2), is 0.58 eV with respect to the VBM. At this condition Cs_i^+ and $\text{V}_{\text{Pb}}^{2-}$ are the dominant atomic point defects,²² and the antisite Pb_{Cs}^+ , to be discussed below, is the most dominant compound defect. The compound vacancy and interstitial defects listed above, are then all stable in the neutral state. A list of the DFEs and concentrations, calculated at the intrinsic Fermi level, of these compound defects is given in Table 1.

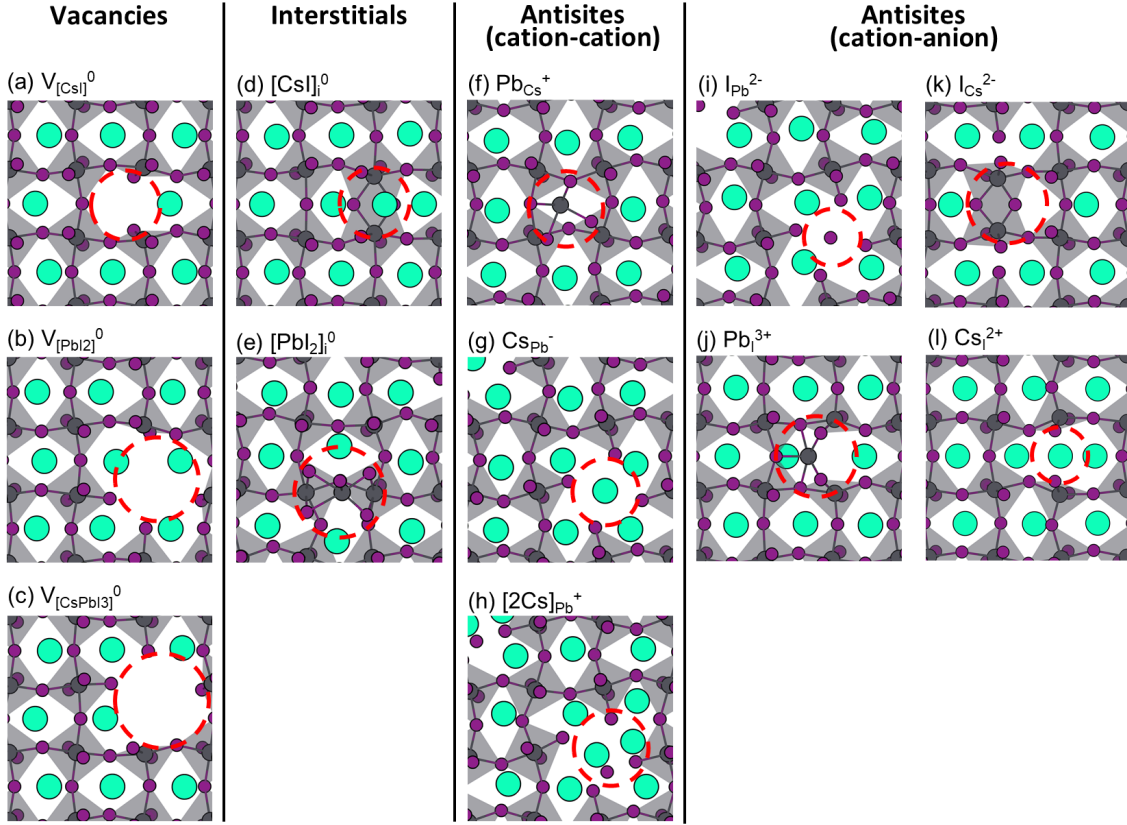


Figure 1: Optimized structures of compound defects in CsPbI_3 in their most stable charge states under intrinsic conditions; (a-c) compound vacancies, (d-e) compound interstitials, (f-h) cation-cation antisites, and (i-l) cation-anion antisites. Cs, Pb and I atoms are represented by green, black and purple circles, respectively, with PbI octahedra colored gray. The positions of the compound defects are indicated by the red circles.

A compound vacancy defect creates a considerable hole in the lattice, see Figures 1(a-c), and its DFE is correspondingly high. The vacancy V_{PbI_2} is relatively easiest to form, with a DFE of 1.12 eV, followed by V_{CsI} and $\text{V}_{[\text{CsPbI}_3]}$, whose DFEs are 1.35 eV and 1.81 eV,

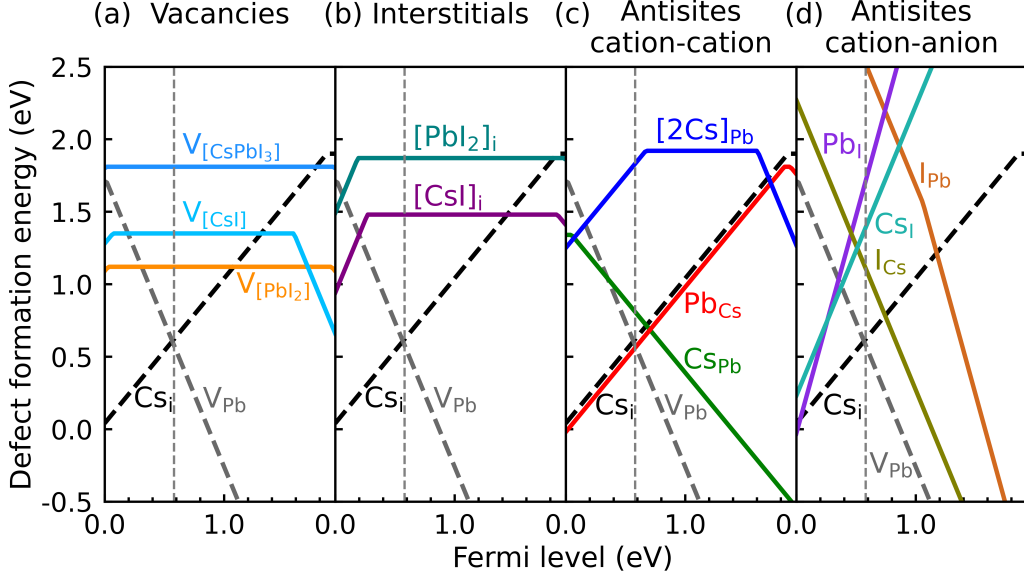


Figure 2: Formation energies of compound defects as a function of the Fermi level; (a) vacancies, (b) interstitials, (c) cation-cation antisites, and (d) cation-anion antisites. For comparison, the dashed black lines represent the formation energies of the two dominant point defects in CsPbI_3 . The intrinsic Fermi level, determined by the charge neutrality condition, Eq. (2), is indicated by the vertical dashed gray line.

respectively. All of these numbers are $\gtrsim 0.5$ eV higher than the DFEs of the simple point defects Cs_i^+ and $\text{V}_{\text{Pb}}^{2-}$, which means that concentration of compound vacancy defects is negligible at room temperature under equilibrium conditions (Table 1).

Compound interstitial defects, $[\text{CsI}]_i$ and $[\text{PbI}_2]_i$, can be accommodated in the CsPbI_3 lattice by a distortion or tilting of the Pb-I octahedra, see Figures 1(d,e), albeit at a considerable energy penalty, with DFEs of 1.48 eV and 1.87 eV, respectively. We conclude that compound interstitial defects also have negligible concentrations at room temperature under equilibrium conditions, see Table 1.

Turning to antisite defects, as there are two different cations in CsPbI_3 , antisites can be formed among cations, i.e., by a cation of one type occupying a position of a cation of the other type, Pb_{Cs} (Pb substitutes Cs), or Cs_{Pb} , see Figures 1(f, g). We stick to the nomenclature of antisites, but note that replacing one cation by another can lead to a notable local distortion of the lattice, such that the substituting ion is significantly displaced from

the lattice position of the original ion. Pb ions are nominally 2+, and Cs ions are 1+, so it is not surprising to find the most stable charge states of these antisites as Pb_{Cs}^+ and Cs_{Pb}^- . The DFE of Pb_{Cs}^+ is comparable to that of the simple point defects Cs_i^+ and $\text{V}_{\text{Pb}}^{2-}$, see Figure 2(c) and Table 1, which means that this antisite occurs relatively frequently under equilibrium conditions. The Cs_{Pb}^- antisite defect has a DFE that is ~ 0.25 eV larger than that of Pb_{Cs}^+ , making it less favorable.

Table 1: Formation energies (ΔH_f) and concentrations of compound defects under equilibrium conditions ($c_{\text{equilibrium}}$, $T = 300\text{K}$); recombination reactions, recombination energies (ΔH_r) and concentrations of compound defects under nonequilibrium conditions ^a ($c_{\text{nonequilibrium}}$), all at the intrinsic Fermi level.

Defects	ΔH_f (eV)	$c_{\text{equilibrium}}$ (cm^{-3})	Reaction	ΔH_r (eV)	$c_{\text{nonequilibrium}}$ (cm^{-3})
<u>Vacancies</u>					
V_{CsI}^0	1.35	2.81×10^{-1}	$\text{V}_{\text{Cs}}^- + \text{V}_I^+$	-0.06	7.75×10^8
$\text{V}_{\text{PbI}_2}^0$	1.12	7.23×10^2	$\text{V}_{\text{Pb}}^{2-} + 2\text{V}_I^+$	-0.83	5.26×10^{14}
$\text{V}_{\text{CsPbI}_3}^0$	1.81	1.73×10^{-9}	$\text{V}_{\text{Cs}}^- + \text{V}_{\text{Pb}}^{2-} + 3\text{V}_I^+$	-1.54	5.10×10^{13}
<u>Interstitials</u>					
$[\text{CsI}]_i^0$	1.48	1.51×10^{-3}	$\text{Cs}_i^+ + \text{I}_i^-$	0.16	1.41×10^6
$[\text{PbI}_2]_i^0$	1.87	1.09×10^{-9}	$\text{Pb}_i^{2+} + 2\text{I}_i^-$	-0.30	3.24×10^5
<u>Antisites (cation-cation)</u>					
Pb_{Cs}^+	0.56	1.71×10^{12}	$\text{Pb}_i^{2+} + \text{V}_{\text{Cs}}^-$	-0.93	9.44×10^{15}
Cs_{Pb}^-	0.81	1.09×10^8	$\text{Cs}_i^+ + \text{V}_{\text{Pb}}^{2-}$	-0.39	3.88×10^{15}
$[\text{2Cs}]_{\text{Pb}}^+$	1.83	7.72×10^{-10}	$2\text{Cs}_i^+ + \text{V}_{\text{Pb}}^{2-} + e^+$	0.01	1.51×10^3
<u>Antisites (cation-anion)</u>					
$\text{I}_{\text{Pb}}^{2-}$	2.51	2.90×10^{-21}	$\text{I}_i^- + \text{V}_{\text{Pb}}^{2-} + e^+$	1.24	1.12×10^{-12}
Pb_I^{3+}	1.72	1.58×10^{-7}	$\text{Pb}_i^{2+} + \text{V}_I^+$	0.25	9.82×10^2
$\text{I}_{\text{Cs}}^{2-}$	1.10	3.50×10^3	$\text{I}_i^- + \text{V}_{\text{Cs}}^-$	-0.31	1.10×10^{13}
Cs_I^{2+}	1.40	4.39×10^{-2}	$\text{Cs}_i^+ + \text{V}_I^+$	0.08	3.28×10^7

^a The specific nonequilibrium conditions are defined by defect formation at an elevated temperature equilibrium at $T = 500\text{K}$, followed by allowing for recombination through isolation at $T = 300\text{K}$.

In principle it is possible that a Pb vacancy, $\text{V}_{\text{Pb}}^{2-}$, captures two Cs^+ ions to form the $[\text{2Cs}]_{\text{Pb}}$ antisite, see Figure 1(h). Somewhat surprisingly, the most stable charge state at the intrinsic Fermi level of this antisite is $[\text{2Cs}]_{\text{Pb}}^+$. Its DFE is, however, $\gtrsim 1$ eV larger than that of the Cs_{Pb}^- antisite, demonstrating that it is difficult to plant two Cs ions in one Pb lattice position, see Figures 1(g) and (h).

A second possible type of antisite results from placing an anion on a cation position, or vice versa. There are four possibilities, see Figures 1(i-l). Again we maintain the nomenclature of antisites, but note that the replacing anion or cation typically does not occupy a lattice site. For instance, in the I_{Cs} antisite the I ion does not replace the Cs ion at its lattice position, Figure 1(k). Instead, it forms a Pb-I-Pb bridge bond nearby, which is a typical bonding configuration for I interstitials.²² In this sense, an antisite is actually a bonding configuration between a vacancy and an interstitial.

The most stable charge states of these antisites can be guessed from summing the charges of the point defects that can recombine to these antisites. For instance, Cs_I^{2+} and Pb_I^{3+} antisites originate from recombining Cs_i^+ , respectively Pb_i^{2+} interstitials with V_I^+ vacancies, whereas the I_{Cs}^{2-} antisite results from recombining an I_i^- interstitial with a V_{Cs}^- vacancy. I_{Pb}^{2-} is an exception to this rule; it might be a recombination between an I_i^0 interstitial and a V_{Pb}^{2-} vacancy. In general, cation-anion antisites lead to unusually high charge states for the defects inserted into the $CsPbI_3$ lattice, Figures 1 (i-l). This might in part explain their large DFEs, where all cation-anion antisite defects have a DFE that is at least 0.5 eV larger than that of simple point defects, Figure 2 and Table 1.

In summary, under equilibrium conditions at room temperature, only the formation of cation(Cs)-cation(Pb) antisites is prominent, with Pb_{Cs}^+ presenting a comparable concentration to those of the dominant point defects Cs_i^+ and V_{Pb}^{2-} , and Cs_{Pb}^- is formed to a lesser extent. Other compound defects, antisites, compound vacancies or interstitials, are not favorable due to their large DFEs.

Nonequilibrium Conditions

Defect concentrations can change drastically under nonequilibrium conditions. Highly nonequilibrium conditions typically occur during the growth of the perovskite crystals. The resulting concentration of defects can then not be simply deduced from the equilibrium relation, Eq. (1). The types and concentrations of defects that occur of course depend on the exact

growth conditions. To estimate the potential role played by compound defects, we explore the following model.

It starts from the assumption that initially defects are created at an elevated temperature, which could reflect an annealing step during the growth process, for instance, with concentrations that can be estimated from Eq. (1). The crystal is then brought to room temperature, where the point defects and compound defects present are allowed to recombine or dissociate, according to Eq. (8), under the constraints of conservation of the total number of atoms in the defects, Eq. (10).

A key parameter determining the recombination reaction is the reaction energy, Eq. (9). Table 1 shows the reaction energies, calculated at the intrinsic Fermi level, of the recombination reactions that lead to the compound defects, and Figure 3(a) shows the reaction energies as a function of the Fermi level. For a recombination reaction to lead to an appreciable concentration of a compound defect, its reaction energy needs to be significantly negative.

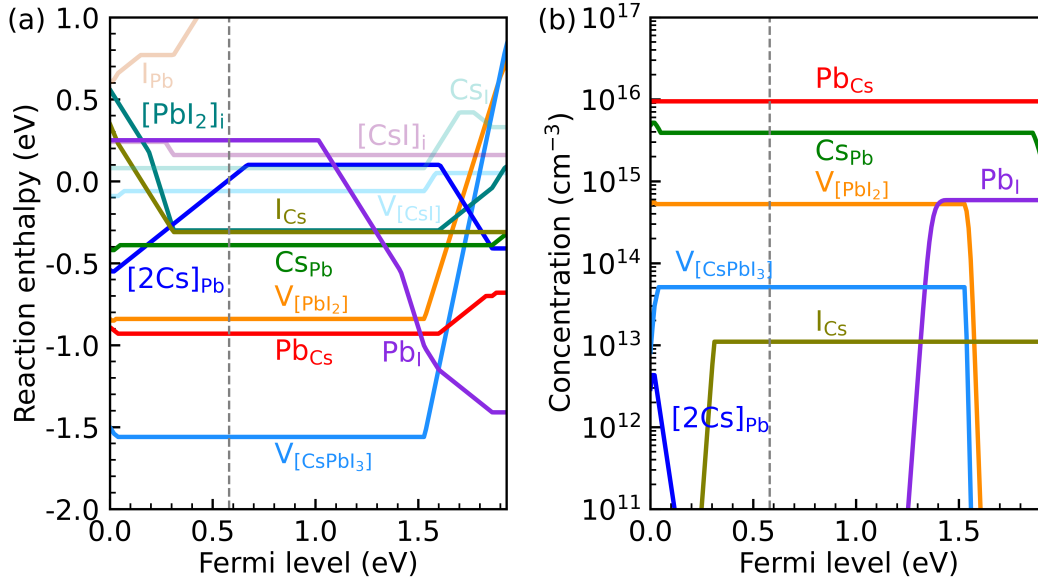


Figure 3: (a) Reaction energies of compound defects, Eq. (9), as a function of the Fermi level; (b) Concentrations under nonequilibrium conditions, resulting from the law of mass action at room temperature, Eqs. (8) and (10), with the initial concentrations of defects determined by equilibrium at $T = 500K$. The intrinsic Fermi level is indicated by the vertical dashed gray line.

Figure 3(a) and Table 1 show that at the intrinsic Fermi level this is the case for the compound vacancies $V_{[\text{CsPbI}_3]}^0$ and $V_{\text{PbI}_2}^0$ and the antisite Pb_{Cs}^+ , with reaction energies in the range of -0.8 to -1.5 eV. The antisites Cs_{Pb}^- and $\text{I}_{\text{Cs}}^{2-}$, as well as the compound interstitial $[\text{PbI}_2]_i^0$ have a moderately negative reaction energy between -0.3 and -0.4 eV, whereas that of the compound vacancy V_{CsI}^0 is marginally small. The reaction energies of other compound defects, anion-cation antisites (except the mentioned $\text{I}_{\text{Cs}}^{2-}$) and the double antisite $[2\text{Cs}]_{\text{Pb}}^+$, or the compound interstitial $[\text{CsI}]_i^0$, are positive, which means that these complexes are not formed in significant concentrations.

However, merely having a negative reaction energy does not imply that a compound defect will form in an appreciable concentration, as formation of a complex necessarily involves a decrease in entropy. Using the law of mass action, Eq. (8), which is based upon free energies, the effects of entropy are included. At room temperature equilibrium conditions, the most prominent point defects are the Pb vacancy V_{Pb}^{2-} and the Cs interstitial Cs_i^+ , with concentrations of $1.11 \times 10^{12} \text{ cm}^{-3}$, $5.03 \times 10^{11} \text{ cm}^{-3}$, respectively.²² Under those conditions, all compound defects have a concentration that is at least three orders of magnitude lower, see Figure S1 of the Supporting Information, which means that the loss of entropy involved in their formation reaction essentially prohibits the occurrence of compound defects. The antisite defect Pb_{Cs}^+ is an exception, which forms in a large concentration of $1.71 \times 10^{12} \text{ cm}^{-3}$ resulting from its low formation energy rather than the recombination of point defects.

At $T = 500$ K the concentrations of the most prominent point defects, V_{Pb}^{2-} and Cs_i^+ , and the cation-cation antisite Pb_{Cs}^+ are raised to $\sim 10^{16} \text{ cm}^{-3}$, see Figure S2 and Table S2 of the Supporting Information. Based on these initial conditions, the concentrations of compound defects at $T = 300$ K (and intrinsic Fermi level, Eq. (2)), according to Eqs. (8) and (10), are shown in Figure 3(b). Most noticeable under these circumstances is that the two cation point defects recombine to form the antisite Cs_{Pb}^- in a large concentration of $3.88 \times 10^{15} \text{ cm}^{-3}$.

A third relatively prominent defect is the compound vacancy $V_{[\text{PbI}_2]}^0$ with a concentration

of $5.26 \times 10^{14} \text{ cm}^{-3}$. The compound vacancy $V_{[\text{CsPbI}_3]}^0$ and the anion-cation antisite $\text{I}_{\text{Cs}}^{2-}$ occur at lower concentrations of $5.10 \times 10^{13} \text{ cm}^{-3}$ and $1.10 \times 10^{13} \text{ cm}^{-3}$, respectively, whereas the concentrations of the other compound defects are much smaller (under intrinsic Fermi level conditions).

In summary, whereas at equilibrium conditions compound defects are unlikely to form at room temperature, creation of point defects at elevated temperatures and subsequent annealing leads to recombination of point defects, and a prominent appearance of cation-cation antisites Pb_{Cs}^+ and Cs_{Pb}^- . Less important, though still present in appreciable quantities, are the compound vacancies $V_{[\text{PbI}_2]}$ and $V_{[\text{CsPbI}_3]}$, and the anion-cation antisite $\text{I}_{\text{Cs}}^{2-}$.

Shifting the Fermi Level

Nonequilibrium conditions of a different type occur when operating perovskite solar cells. Electrons and holes are produced by light absorption, creating quasi-Fermi levels for electrons and holes that are closer to the band edges than the intrinsic Fermi. The DFEs, Eq. (3), and therefore the defect concentrations, Eq. (1), are affected by the position of the Fermi level, depending on the charge states of the defects.

As can be observed in Figures 2(a,b), the compound vacancies and interstitials maintain their neutral states (and their DFEs) over a large range of Fermi level positions. Only if the Fermi level is close to the conduction band minimum (CBM) does V_{CsI} become negatively charged, and if the Fermi level is close to the valence band maximum (VBM), $[\text{CsI}]_i$ and $[\text{PbI}_2]_i$ become positively charged.

The cation-cation antisite $[2\text{Cs}]_{\text{Pb}}$, which is positively charged at the intrinsic Fermi level, Figure 2(c), becomes neutral upon raising the Fermi level, and becomes negatively charged for a Fermi level close to the CBM. The other cation-cation antisites behave similar to simple (charged) point defects, with Pb_{Cs}^+ decreasing its DFE upon lowering the Fermi level, and Cs_{Pb}^- decreasing its DFE upon raising the Fermi level.

The DFEs of the highly charged cation-anion antisites of course depend strongly on the

position of the Fermi level, Figure 2(d), the Cs_I^{2+} and Pb_I^{3+} antisites becoming favorable for Fermi level positions close to the VBM, and the $\text{I}_{\text{Cs}}^{2-}$ and $\text{I}_{\text{Pb}}^{3-}$ becoming more important for Fermi levels close to the CBM.

At the intrinsic Fermi level, or indeed for a Fermi level positioned anywhere in the midgap region, we find that the most stable charge state of a compound defect is simply the sum of the charges of the point defects involved in the recombination reaction, Eq. (4),

$$\alpha_1 q_1 + \dots + \alpha_m q_m = \beta q_B \quad (12)$$

As long as this holds, the reaction energy does not depend on the exact position of the Fermi level and is constant, see Eqs. (3) and (9), which can be observed in Figure 3(a) and Figure S3 of the Supporting Information. Consequently, for a Fermi level in this range, the concentrations of the compound defects do not depend upon the exact position of the Fermi level, see Figure 3(c).

If the Fermi level is close to the band edges, defects change their charge states, as discussed above. In fact, charge conservation, Eq. (12) does not necessarily hold, as it becomes energetically more advantageous to accept holes or electrons from the valence or conduction bands by one or more of the defects involved in the reaction. Figure 3(a) shows that, as a result of this, reaction energies can change significantly if the Fermi level comes closer to the band edges. As an example, the reaction energy of $[\text{2Cs}]_{\text{Pb}}$ decreases if the Fermi level either is close to the VBM or close to the CBM, where this compound defect becomes positively ($[\text{2Cs}]_{\text{Pb}}^+$), respectively negatively ($[\text{2Cs}]_{\text{Pb}}^{2-}$) charged.

Most remarkable in Figure 3(a) is the strong decrease of the reaction energy of the cation-anion antisite Pb_I if the Fermi level moves upwards from 1.01 eV. At the intrinsic Fermi level, this compound defect is highly charged, Pb_I^{3+} , Figure 2(d), but upon raising the Fermi level, it becomes energetically advantageous to capture one or more electrons from the conduction band, and lower its reaction energy. Further noticeable is the strong increase of the reaction

energies of the compound vacancies $V_{[\text{PbI}_2]}$ and $V_{[\text{CsPbI}_3]}$ for Fermi levels close to the CBM, and for the antisite I_{Cs} and compound interstitial $[\text{PbI}_2]_i$ for a Fermi level close to the VBM. A detailed description of the reaction and defect formation energies of each compound defect is given in Figure S3 of the Supporting Information.

These changes of the reaction energies upon moving the Fermi level closer to the band edges, have consequences for the defect concentrations, Figure 3(b). The cation-cation antisites Pb_{Cs} and Cs_{Pb} remain the dominant defect, but for a Fermi level close to the CBM ($E_F > 1.6$ eV), the concentration of the compound vacancies $V_{[\text{PbI}_2]}$ and $V_{[\text{CsPbI}_3]}$, which are third and fourth most important defects at midgap Fermi level positions, become negligible. The cation-anion antisite Pb_i becomes the third most important defect for $E_F > 1.3$ eV. For a Fermi level closer to the VBM not much happens, unless $E_F < 0.1$ eV, where the antisite $[2\text{Cs}]_{\text{Pb}}$ begins to appear in non-negligible concentrations, while the anion-cation antisite I_{Cs} concentration becomes negligible.

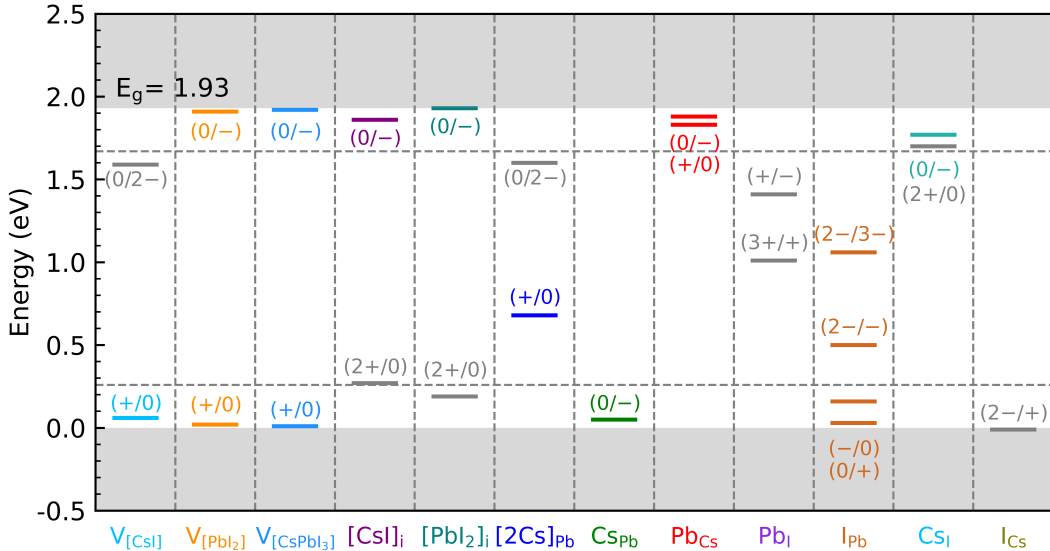


Figure 4: Charge state transition levels of compound defects in CsPbI₃. The levels representing a change of a single $\pm e$ are indicated by colored lines. The bottom and top gray areas represent the valence and conduction bands (calculated with the SCAN+rVV10 functional without spin-orbit coupling). The two horizontal dashed lines are 10 $k_B T$ ($T = 300\text{K}$) above the VBM and below the CBM, respectively.

Charge State Transition Levels

Based on Figure 2 and Eq. (11), the CSTLs of compound defects are determined. The results for all defects considered in this paper, are shown in Figure 4. The most prominent compound defect, the cation-cation antisite Pb_{Cs} , leads to double shallow donor levels, whereas the antisite Cs_{Pb} only leads to a shallow acceptor level. The compound vacancies $V_{[\text{PbI}_2]}$ and $V_{[\text{CsPbI}_3]}$ have both a shallow donor, as well as a shallow acceptor level. The anion-cation antisite I_{Cs} has no levels inside the band gap.

At the intrinsic Fermi level, or indeed if the Fermi level is well inside the band gap, these are all compound defects that can occur in appreciable quantities, see Figure 3(b). If the Fermi level is close to the CBM, the concentration of Pb_{I} antisites increases. Although this antisite introduces two deep levels inside the band gap, both of these levels involve a change in charge state of two electrons, i.e., $3+/1+$ and $+/-$. These levels are likely to be much less active than donor or acceptor levels associated with a change of one in charge state, as the probability of trapping two electrons simultaneously is very low.^{19,36} If the Fermi level becomes extremely close to the VBM, the concentration of $[\text{2Cs}]_{\text{Pb}}$ becomes non-negligible. As its CSTL ($+/0$) is well inside the band gap, this compound defect forms a deep trap, which can act as a harmful recombination center.

Besides the defects discussed in the previous two paragraphs, all other defects occur in such negligible quantities, that their electronic impact is negligible. In fact, the only compound defect considered in this paper that forms a series of deep trap levels, which is the anion-cation antisite I_{Pb} , Figure 3(b), has a very large positive reaction energy, Table 1, so it does not form under practical conditions.

In summary, the relatively abundant compound defects either form shallow donor or acceptor levels (Pb_{Cs} , Cs_{Pb} , $V_{[\text{PbI}_2]}$, $V_{[\text{CsPbI}_3]}$, I_{Cs} ,) or electronically not very active levels (Pb_{I}). Only under relatively extreme conditions, with a Fermi level very close to the VBM, the compound defect $[\text{2Cs}]_{\text{Pb}}$ can form, which has a deep trap level.

Conclusions

To conclude, we have studied the formation of compound defects in the archetype inorganic halide perovskite CsPbI₃ by means of DFT calculations using the accurate and efficient SCAN+rVV10 functional. Considering compound vacancies, $V_{[\text{CsI}]}$, $V_{[\text{PbI}_2]}$, and $V_{[\text{CsPbI}_3]}$, compound interstitials $[\text{CsI}]_i$ and $[\text{PbI}_2]_i$, cation-cation antisites, Pb_{Cs} , Cs_{Pb} , $[2\text{Cs}]_{\text{Pb}}$, and anion-cation antisites I_{Cs} , I_{Pb} , Cs_{I} , Pb_{I} , we evaluate their formation under equilibrium conditions, and under conditions that reflect their formation as recombination reactions of simple point defects.

Although the energies of several of these recombination reactions are favorable, under equilibrium conditions at room temperature, only the formation of the antisite where Pb substitutes Cs is prominent, and the concentrations of point defects are too small to give any appreciable amount of other compound defects. However, under nonequilibrium conditions, mimicked by a high temperature annealing step, several types of compound defects can be formed in significant concentrations. Most prominent are the cation-cation antisites Pb_{Cs}^+ and Cs_{Pb}^- , with concentrations comparable to those of the dominant point defects Cs_i^+ and V_{Pb}^{2-} . Smaller amounts of the compound vacancies $V_{[\text{PbI}_2]}^0$ and $V_{[\text{CsPbI}_3]}^0$, and the anion-cation antisite $\text{I}_{\text{Cs}}^{2-}$ can be observed, whereas the concentrations of other defects are negligible.

Under solar cell operating conditions the (quasi) Fermi level can shift to the proximity of the VBM and CBM, which promotes the formation of certain compound defects, and suppresses that of others. If the Fermi level is close to the CBM, the formation of $V_{[\text{PbI}_2]}^0$ and $V_{[\text{CsPbI}_3]}^0$ is suppressed, and that of the cation-anion antisite Pb_{I}^- is promoted, whereas if the Fermi level is close to the VBM, the formation of $\text{I}_{\text{Cs}}^{2-}$ is suppressed, and that of $[2\text{Cs}]_{\text{Pb}}^+$ is promoted. The other defects are less affected by a change in Fermi level.

The antisites and compound vacancies that can occur in appreciable concentrations (Pb_{Cs} , Cs_{Pb} , I_{Cs} , $V_{[\text{PbI}_2]}$ and $V_{[\text{CsPbI}_3]}$) create shallow trap levels only. The antisite Pb_{I} creates several deep levels, which are, however, not very active electronically, as their charge state

transition involves the arrival of two electrons simultaneously. Only the compound defect $[2\text{Cs}]_{\text{Pb}}$ leads to a deep trap level. However, as discussed above, this defect is only likely to form if the Fermi level is very close to the VBM. These results illustrate the exemplary electronic tolerance of halide perovskites towards the presence of defects.

Acknowledgement

H.X. acknowledges funding from the China Scholarship Council (CSC, No. 201806420038). S.T. acknowledges funding from the Computational Sciences for Energy Research (CSER) tenure track program of Shell and NWO (Project No. 15CST04-2) and the NWO START-UP grant from the Netherlands.

Supporting Information Available

A list of number of possible defect sites and counting rule for each compound defect; Concentration of compound defects at 300 K; Temperature dependence of concentrations of point defects; Table of concentrations of point defects at 300 K and 500 K; Detailed comparison of reaction energies and formation energies of each compound defect.

References

- (1) National Renewable Energy Laboratory, Best Research-Cell Efficiency Chart. 2022; <https://www.nrel.gov/pv/cell-efficiency.html>.
- (2) Kim, H. S.; Seo, J. Y.; Park, N. G. Material and Device Stability in Perovskite Solar Cells. *ChemSusChem* **2016**, *9*, 2528–2540.
- (3) Zhou, Y.; Zhao, Y. Chemical stability and instability of inorganic halide perovskites. *Energy Environ. Sci.* **2019**, *12*, 1495–1511.

- (4) Park, B.-w.; Seok, S. I. Intrinsic Instability of Inorganic–Organic Hybrid Halide Perovskite Materials. *Adv. Mater.* **2019**, *31*, 1805337.
- (5) He, S.; Qiu, L.; Ono, L. K.; Qi, Y. How far are we from attaining 10-year lifetime for metal halide perovskite solar cells? *Mater. Sci. Eng. R Reports* **2020**, *140*, 100545.
- (6) Yuan, Y.; Huang, J. Ion Migration in Organometal Trihalide Perovskite and Its Impact on Photovoltaic Efficiency and Stability. *Acc. Chem. Res.* **2016**, *49*, 286–293.
- (7) Yang, J.-H.; Yin, W.-J.; Park, J.-S.; Wei, S.-H. Fast self-diffusion of ions in $\text{CH}_3\text{NH}_3\text{PbI}_3$: the interstitially mechanism versus vacancy-assisted mechanism. *J. Mater. Chem. A* **2016**, *4*, 13105–13112.
- (8) Eames, C.; Frost, J. M.; Barnes, P. R. F.; O’Regan, B. C.; Walsh, A.; Islam, M. S. Ionic transport in hybrid lead iodide perovskite solar cells. *Nat. Commun.* **2015**, *6*, 7497.
- (9) Azpiroz, J. M.; Mosconi, E.; Bisquert, J.; De Angelis, F. Defect migration in methylammonium lead iodide and its role in perovskite solar cell operation. *Energy Environ. Sci.* **2015**, *8*, 2118–2127.
- (10) Pols, M.; Vicent-Luna, J. M.; Filot, I.; van Duin, A. C. T.; Tao, S. Atomistic Insights Into the Degradation of Inorganic Halide Perovskite CsPbI_3 : A Reactive Force Field Molecular Dynamics Study. *J. Phys. Chem. Lett.* **2021**, *12*, 5519–5525.
- (11) Mosconi, E.; Azpiroz, J. M.; Angelis, F. D. Ab Initio Molecular Dynamics Simulations of Methylammonium Lead Iodide Perovskite Degradation by Water. *Chem. Mater.* **2015**, *27*, 4885–4892.
- (12) Aristidou, N.; Eames, C.; Sanchez-Molina, I.; Bu, X.; Kosco, J.; Islam, M. S.; Haque, S. A. Fast oxygen diffusion and iodide defects mediate oxygen-induced degradation of perovskite solar cells. *Nat. Commun.* **2017**, *8*, 15218.

- (13) Tan, S.; Yavuz, I.; Weber, M. H.; Huang, T.; Chen, C. H.; Wang, R.; Wang, H. C.; Ko, J. H.; Nuryyeva, S.; Xue, J. et al. Shallow Iodine Defects Accelerate the Degradation of α -Phase Formamidinium Perovskite. *Joule* **2020**, *4*, 2426–2442.
- (14) Barker, A. J.; Sadhanala, A.; Deschler, F.; Gandini, M.; Senanayak, S. P.; Pearce, P. M.; Mosconi, E.; Pearson, A. J.; Wu, Y.; Srimath Kandada, A. R. et al. Defect-Assisted Photoinduced Halide Segregation in Mixed-Halide Perovskite Thin Films. *ACS Energy Lett.* **2017**, *2*, 1416–1424.
- (15) de Walle, C. G. V.; Neugebauer, J. First-principles calculations for defects and impurities: Applications to III-nitrides. *J. Appl. Phys.* **2004**, *95*, 3851–3879.
- (16) Freysoldt, C.; Grabowski, B.; Hickel, T.; Neugebauer, J.; Kresse, G.; Janotti, A.; Van de Walle, C. G. First-principles calculations for point defects in solids. *Rev. Mod. Phys.* **2014**, *86*, 253–305.
- (17) Yin, W.-J.; Shi, T.; Yan, Y. Unusual defect physics in CH₃NH₃PbI₃ perovskite solar cell absorber. *Appl. Phys. Lett.* **2014**, *104*, 63903.
- (18) Shi, T.; Yin, W.-J.; Hong, F.; Zhu, K.; Yan, Y. Unipolar self-doping behavior in perovskite CH₃NH₃PbBr₃. *Appl. Phys. Lett.* **2015**, *106*, 103902.
- (19) Meggiolaro, D.; De Angelis, F. First-Principles Modeling of Defects in Lead Halide Perovskites: Best Practices and Open Issues. *ACS Energy Lett.* **2018**, *3*, 2206–2222.
- (20) Huang, Y.; Yin, W.-J.; He, Y. Intrinsic Point Defects in Inorganic Cesium Lead Iodide Perovskite CsPbI₃. *J. Phys. Chem. C* **2018**, *122*, 1345–1350.
- (21) Meggiolaro, D.; Mosconi, E.; De Angelis, F. Formation of Surface Defects Dominates Ion Migration in Lead-Halide Perovskites. *ACS Energy Lett.* **2019**, *4*, 779–785.
- (22) Xue, H.; Brocks, G.; Tao, S. Intrinsic defects in primary halide perovskites: A first-principles study of the thermodynamic trends. *Phys. Rev. Mater.* **2022**, *6*, 055402.

- (23) Xue, H.; Brocks, G.; Tao, S. First-principles calculations of defects in metal halide perovskites: A performance comparison of density functionals. *Phys. Rev. Mater.* **2021**, *5*, 125408.
- (24) Kye, Y. H.; Yu, C. J.; Jong, U. G.; Chen, Y.; Walsh, A. Critical Role of Water in Defect Aggregation and Chemical Degradation of Perovskite Solar Cells. *J. Phys. Chem. Lett.* **2018**, *9*, 2196–2201.
- (25) Kim, J.; Lee, S.-H.; Lee, J. H.; Hong, K.-H. The Role of Intrinsic Defects in Methylammonium Lead Iodide Perovskite. *J. Phys. Chem. Lett.* **2014**, *5*, 1312–1317.
- (26) Keeble, D. J.; Wiktor, J.; Pathak, S. K.; Phillips, L. J.; Dickmann, M.; Durose, K.; Snaith, H. J.; Egger, W. Identification of lead vacancy defects in lead halide perovskites. *Nat. Commun.* **2021**, *12*, 1–7.
- (27) Agiorgousis, M. L.; Sun, Y.-Y.; Zeng, H.; Zhang, S. Strong Covalency-Induced Recombination Centers in Perovskite Solar Cell Material CH₃NH₃PbI₃. *J. Am. Chem. Soc.* **2014**, *136*, 14570–14575.
- (28) Pols, M.; Hilpert, T.; Filot, I.; van Duin, A. C. T.; Calero, S.; Tao, S. What Happens at Surfaces and Grain Boundaries of Halide Perovskites: Insights from Reactive Molecular Dynamics Simulations of CsPbI₃. 2022; <https://arxiv.org/abs/2205.10545v1>.
- (29) Kresse, G.; Hafner, J. Ab initio molecular dynamics for liquid metals. *Phys. Rev. B* **1993**, *47*, 558–561.
- (30) Kresse, G.; Furthmüller, J. Efficient iterative schemes for ab initio total-energy calculations using a plane-wave basis set. *Phys. Rev. B* **1996**, *54*, 11169–11186.
- (31) Kresse, G.; Furthmüller, J. Efficiency of ab-initio total energy calculations for metals and semiconductors using a plane-wave basis set. *Comput. Mater. Sci.* **1996**, *6*, 15–50.

- (32) Peng, H.; Yang, Z.-H.; Perdew, J. P.; Sun, J. Versatile van der Waals Density Functional Based on a Meta-Generalized Gradient Approximation. *Phys. Rev. X* **2016**, *6*, 41005.
- (33) Komsa, H. P.; Rantala, T. T.; Pasquarello, A. Finite-size supercell correction schemes for charged defect calculations. *Phys. Rev. B* **2012**, *86*, 045112.
- (34) Wiktor, J.; Rothlisberger, U.; Pasquarello, A. Predictive Determination of Band Gaps of Inorganic Halide Perovskites. *J. Phys. Chem. Lett.* **2017**, *8*, 5507–5512.
- (35) Tao, S.; Schmidt, I.; Brocks, G.; Jiang, J.; Tranca, I.; Meerholz, K.; Olthof, S. Absolute energy level positions in tin- and lead-based halide perovskites. *Nat. Commun.* **2019**, *10*, 2560.
- (36) Tress, W. Perovskite Solar Cells on the Way to Their Radiative Efficiency Limit – Insights Into a Success Story of High Open-Circuit Voltage and Low Recombination. *Advanced Energy Materials* **2017**, *7*, 1602358.

Graphical TOC Entry

